Validation of a semiautomatic image analysis software for the quantification of musculoskeletal tissues

Mahdi Imani
The University of Melbourne
Ebrahim Bani Hassan
The University of Melbourne
Sara Vogrin
The University of Melbourne
Aaron Samuel Tze Nor Ch'Ng
The University of Melbourne
Nancy E. Lane
University of California at Davis School of Medicine
Jane A. Cauley
University of Pittsburgh
Gustavo Duque (gustavo.duque@unimelb.edu.au)
University of Melbourne https://orcid.org/0000-0001-8126-0637

Method Article

Keywords: Intramuscular fat, image processing, osteoporosis, sarcopenia, osteosarcopenia, marrow adipose tissue

Posted Date: June 24th, 2021

DOI: https://doi.org/10.21203/rs.3.rs-650019/v1

Version of Record: A version of this preprint was published at Calcified Tissue International on September 13th, 2021. See the published version at https://doi.org/10.1007/s00223-021-00914-4.

Abstract

Background: Accurate quantification of bone, muscle, and their components is still an unmet need in the musculoskeletal field. Current methods to quantify tissue volumes in 3D images are expensive, labor-intensive, and time-consuming; thus, a reliable, valid, and quick application is highly needed.

Methods: Tissue Compass is a standalone software for semiautomatic segmentation and automatic quantification of musculoskeletal organs. To validate the software, cross-sectional micro-CT scans images of rat femur (n=19), and CT images of hip and abdomen (n=100) from the Osteoporotic Fractures in Men (MrOS) Study were used to quantify bone, hematopoietic marrow (HBM), and marrow adipose tissue (MAT) using commercial manual software as a comparator. Also, abdominal CT scans (n=100) were used to quantify psoas muscle volumes and intermuscular adipose tissue (IMAT) using the same software. We calculated Pearson's correlation coefficients, individual intra-class correlation coefficients (ICC), and Bland-Altman limits of agreement together with Bland-Altman plots to show the inter- and intra-observer agreement between Tissue Compass and commercially available software.

Results: In the animal study, the agreement between Tissue Compass and commercial software was r>0.93 and ICC>0.93 for rat femur measurements. Bland-Altman limits of agreement was -720.89 (-1.5e+04, 13074.00) for MAT, 4421.11 (-1.8e+04, 27149.73) for HBM and -6073.32 (-2.9e+04, 16388.37) for bone. The inter-observer agreement for QCT human study between two observers was r>0.99 and ICC>0.99. Bland-Altman limits of agreement was 0.01 (-0.07, 0.10) for MAT in hip, 0.02 (-0.08, 0.12) for HBM in hip, 0.05 (-0.15, 0.25) for bone in hip, 0.02 (-0.18, 0.22) for MAT in L1, 0.00 (-0.16, 0.16) for HBM in L1, 0.02 (-0.23, 0.27) for bone in L1. The intra-observer agreement for QCT human study between two applications was r>0.997 and ICC>0.99. Bland-Altman limits of agreement was 0.03 (-0.13, 0.20) for MAT in hip, 0.05 (-0.08, 0.18) for HBM in hip, 0.05 (-0.24, 0.34) for bone in hip, -0.02 (-0.34, 0.31) for MAT in L1, -0.14 (-0.44, 0.17) for HBM in L1, -0.29 (-0.62, 0.05) for bone in L1, 0.03 (-0.08, 0.15) for IMAT in psoas, and 0.02 (-0.35, 0.38) for muscle in psoas.

Conclusion: Compared to a conventional application, Tissue Compass demonstrated high accuracy and non-inferiority while also facilitating easier analyses. Tissue Compass could become the tool of choice to diagnose tissue loss/gain syndromes in the future by requiring a small number of CT sections to detect tissue volumes and fat infiltration.

Introduction

Tissue loss syndromes (i.e. cachexia, osteoporosis, sarcopenia, osteosarcopenia, and frailty) lead to significant changes in the volume and composition of musculoskeletal tissues [1, 2]. Considering the aging world population and the increasing prevalence of comorbidities and sedentary lifestyle, the prevalence of tissue loss syndromes increases while predisposing to adverse outcomes such as falls, fractures, disability, and early mortality [3, 4]. Therefore, early, and accurate diagnosis of these conditions and the prediction of their associated adverse outcomes are crucial.

Although dual-energy X-ray absorptiometry (DXA) is considered the gold standard for the diagnosis of osteoporosis, this method has several pitfalls and limitations [5]. In addition, the use of DXA for the diagnosis of sarcopenia has been recently questioned by the Sarcopenia Definition and Outcomes Consortium (SDOC), in which quantification of appendicular lean mass (ALM) was excluded from their diagnostic algorithms [6]. Nevertheless, these limitations of the DXA do not exclude imaging techniques in general as a reliable diagnostic method for tissue loss syndromes.

Our knowledge of the roles of ectopic fat infiltration in tissue loss is expanding. Causative roles for the marrow adipose tissue (MAT) and intermuscular adipose tissue (IMAT) have been suggested in inducing and aggravating osteoporosis and sarcopenia [7, 8]. In addition to its mass, the fatty tissue distribution pattern in the body is acknowledged as an indicator of its metabolic properties, including the ability to induce general or local lipotoxicity [8, 9]. Hence the assessment of three-dimensional (3D) images of the body is increasingly appreciated in clinical medicine and musculoskeletal research [10], as the two-dimensional systems (such as DXA) are currently incapable of accurately assessing fat infiltration and its geography within organs or diagnose the degree of adiposity (including in non-musculoskeletal tissues, e.g., in fatty liver syndrome).

Computed tomography (CT) scan is one of the main noninvasive 3D imaging methods that presents an excellent view of different organs and their composition. This imaging technique has been widely used in the assessment and study of osteoporosis and sarcopenia [11-13] and to quantify adipose tissue within the muscle, bone [14, 15], and other organs [16]. To our knowledge, several programs are available for image analysis and quantification of musculoskeletal tissues, such as Analyze (Mayo Clinic, Rochester, MN), ImageJ (National Institutes of Health, Bethesda, MD), and SliceOmatic (Tomovision, Montreal, Canada). These programs provide valuable techniques to quantify medical images, but they are primarily manual, making them time-consuming, hard to use, and prone to operator-dependent error.

Hence, we have developed an application with less operator involvement which would be expected to be reliable and easier to use, and with high accuracy in identifying multiple intertwined tissues (such as MAT within bone and IMAT in muscle). Here, we validated Tissue Compass against the leading manual commercial segmentation software (SliceOmatic), which has been widely used to quantify tissues on medical images and is considered an appropriate reference standard method [17-19].

Methods

Image analyses software (Tissue Compass) – Tissue Compass was developed based on MATLAB (version R2019b: MathWorks Inc., Natick, MA), a widely used platform for scientific calculation, simulation, and development of standalone applications. Tissue Compass (Supplemental figure 1) is a standalone desktop application designed to analyze images in DICOM, PNG, TIFF, and JPEG formats generated by CT, MRI, and micro-CT imaging devices. There are specific automatic segmentation techniques for five different study areas, including left and right hip bone, vertebra, other bones, and muscle (Fig. 1). As part of the hip bone segmentation technique, the topological distancing and watershed technique has been used [20], and the canny edge detection technique was used for vertebra segmentation [21] (supplemental video 1). For muscle segmentation (supplemental video 2), thresholding technique was used by selecting a phantom as a reference for muscle, fat, and bone or receiving input from the user for these tissues. In addition, Tissue Compass has a highly interactive graphical user interface (GUI), making it easy to use for operators who are not familiar with image analysis. Also, it provides highly interactive editing tools in case the results from semiautomatic techniques need editing.

Analysis of a CT section could take between 30 and 100 seconds (Supplemental videos 1 and 2); four different tissues can be identified inside the bone or muscle detected by providing Hounsfield unit (HU) values for the tissues, and their volumes are quantified automatically (supplemental video 1 and 2). In addition to semiautomatic segmentation techniques, the user can draw several regions of interest (ROI) on the image to be analyzed separately. Also, a manual labeling option in the software allows the user to label multiple tissues using a highly interactive "brush" in one go (a feature that significantly increases image analysis speed, and to our knowledge, is unique to this tool). Users can assign (mask) different areas inside the labeled ROI to be analyzed separately (Fig. 1 d and e, j and k). Also, the software's excellent 3D visualization feature allows the user to review the labeled areas in colored 3D format and control individual tissues' transparency to make them visible through each other (see-through feature; Fig. 2). This feature is helpful since it gives the user a clear view of the tissues' geometric distribution and their associations. For example, bone transparency can be decreased to various levels to make MAT and hematopoietic bone marrow (HBM) visible in situ (Fig. 2 d and e; h and i), or both bone and HBM can be made transparent to study the 3D distribution of the MAT (Fig. 2 f and j) inside bone or IMAT inside the muscle (Fig. 2 c). These images can be viewed from different angles.

Animal study – To determine the validity of Tissue Compass for the quantification of bone and fat mass versus a gold standard (histology), we performed a reanalysis and comparison between tissue volumes quantified using SliceOmatic in our previous study in male Louvain/c/rqrv (LOU) rats [22]. Considering these findings, we have correlated MAT, HBM, and bone volume fractions calculated by Tissue Compass vs SliceOmatic for n=19 animals using the same rat data.

Human study – Quantitative CT (QCT) images of the first lumbar vertebra (L1 vertebra) and left hip bone (that are conventionally studied for the assessment of bone quality) were analyzed in images obtained from 100 participants of the MrOS Study (website: https://mrosonline.ucsf.edu). In this study, men (n=~6000, 90% white with a mean age 73 ± 6 years) were recruited at six US academic medical centers. To be considered for this study, men must have been aged 65 or older, could walk without the assistance of another person, and not have had bilateral hip replacements [23, 24]. Images were analyzed for both bone and muscle. MAT, HBM, and bone volumes in hip and L1 vertebra bones were quantified using Tissue Compass. Muscle and IMAT were quantified in psoas muscles at the fourth lumbar vertebra (L4) level on QCT images of the same subpopulation.

Image analysis techniques:

Manual segmentation – Using SliceOmatic (*v.*5.0), L1 vertebral bodies (9-15 slices, depending on size) and left hip bone (2 to 5 slices) were manually segmented. For repeatability, only slices that contained both trabecular and cortical bone were analyzed in both ROIs. For psoas muscle segmentation, only a single QCT slice at the L4 level in which the L4 vertebra bone was fully visible was analyzed. The brush function of the software was used to assign each voxel to any of the tissues of interest per their HU. The following HU ranges were used to determine bone and its components: <135 for MAT, 136 to 235 for HBM, and >235 for bone. Also, for muscle labeling, the HU thresholds were <-20 for IMAT, -20 to 115 for muscle.

Semiautomatic segmentation – Semiautomatic segmentation was carried out using Tissue Compass (Fig. 1). There are four main muscle detection steps (Fig. 1 a-e): 1- Setting HU or grayscale thresholds to detect muscle tissues. The software can automatically detect a conventional three-tissue phantom and extrapolate accurate thresholds for muscle from the phantom (Fig. 1 a); 2- Excluding non-target tissues (e.g., abdominal organs in an abdominal CT); 3- Editing ROIs using the highly interactive tools to delete the muscles that are not of interest or choose a particular muscle or group of muscles to be quantified (Fig. 1 b); and 4- Automatic labeling ROI voxels (Fig. 1 c). A video of muscle segmentation is provided as supplemental video 1. Bone segmentation follows three main steps (Fig. 1 f-k): 1- Automatic detection of the ROI (Fig. 1 g); 2- Editing the ROI (which is not required if the image quality is satisfactory) (Fig. 1 g); and 3- Automatic labeling ROI voxels (Fig. 1 h). A video of bone segmentation is provided as supplemental video 2.

To test inter-rater and intra-rater reliability, two trained researchers blinded to the data sources analyzed the images for both animal and human studies. After the segmentation process, the number of slides was matched between the two segmentation techniques to ensure both techniques have assessed identical images. The HU thresholds used in this process are the same as manual segmentation.

Statistical analysis – To examine the agreement between Tissue Compass and SliceOmatic, both programs were used for volumetric analysis of L1 vertebra (vertebral body), left hip, and psoas muscle at L4 level from 100 subjects. The inter-observer reliability was examined for 50 subjects at L1 vertebra (vertebral body) and left hip. For the animal study, a sample of 19 micro-CT scans of rat femur was used to compare the results of Tissue Compass and SliceOmatic.

We calculated Pearson's correlation coefficient, the absolute agreement between the methods using individual intra-class correlation coefficient (two-way mixed-effects model), and Bland-Altman limits of agreement together with Bland-Altman plots. All analyses were conducted using Stata 16.1 software (StataCorp. 2019. Stata Statistical Software: Release 16. College Station, TX: StataCorp LLC.).

Results

Animal Micro-CT study – Table 1 shows the agreement between Tissue Compass and SliceOmatic with r>0.93 and intra-class correlation coefficient>0.93 for rat femur measurements. In supplemental figure 2, Bland-Altman plots illustrate the agreement between Tissue Compass and SliceOmatic for rat femur bone measurements.

Human QCT study:

Inter-observer reliability (comparison of two investigators using Tissue Compass) – Table 2 shows the agreement between two investigators using Tissue Compass with r>0.99 and intra-class correlation coefficient>0.99. In Figure 3, Bland-Altman plots illustrate the agreement between the two investigators for bone measurements in the L1 vertebra and left hip.

Intra-observer reliability (comparison between Tissue Compass vs SliceOmatic) – Table 3 shows the agreement between Tissue Compass and SliceOmatic measured by one investigator with r>0.997 and intra-class correlation coefficient>0.99. In Figure 4, Bland-Altman plots illustrate the agreement between Tissue Compass and SliceOmatic for bone and muscle measurements, respectively.

Discussion

This validation study demonstrated that Tissue Compass showed non-inferiority and very similar validity, inter-observer, and intra-observer reliability compared to commercially available image analyses software (SliceOmatic) regularly used to quantify tissue volumes in the musculoskeletal system [8,17,18]. We have

used micro-CT and QCT images to validate our software. The micro-CT validation study was performed in rat femur with excellent agreement between Tissue Compass and SliceOmatic. The QCT intra-observer validation was conducted in the L1 vertebra, left hip, and psoas muscle (L4 level), in which the agreement was near perfect. The QCT inter-observer validation was conducted by two investigators using Tissue Compass at separate times for 50 patients in the L1 vertebra and left hip with almost identical results.

Tissue Compass was designed to overcome several issues previously identified in other image analysis applications, including the ability to analyze a sequence of multiple slides simultaneously, providing volumetric results and mean, maximum, and minimum pixel values for each tissue inside the detected ROI. By creating an easy-to-use and fast application to detect the most commonly used tissues of interest semi-automatically and automatically and quantifying multiple tissues inside selected ROI, we have simplified the image analysis process to facilitate the diagnosis of tissue loss syndromes.

A single-step 3D visualization of tissues and adjusting their transparency to see them through each other to study their spatial association is another advantage of Tissue Compass (Fig. 2). The highly interactive GUI of Tissue Compass has been designed to enable image adjustments and analysis by the minimally trained operator. We successfully trained three image-processing-naive operators in less than 30 minutes each for bone analyses to confirm this. Tissue Compass implements different well-known automatic and semiautomatic segmentation techniques in its segmentation process. Watershed, edge detection, and thresholding are a few techniques used in the software. In addition, Tissue Compass benefits from highly interactive editing tools and a more advanced manual segmentation tool than SliceOmatic.

It has been shown that fat and bone volume are inversely correlated in human and animal studies [25-27]. Fat infiltration of bone marrow can have detrimental effects on bone, induce osteoporosis, and increase the chance of adverse outcomes such as fractures in older adults [28]. Therefore, marrow fat can be used as a diagnostic and therapeutic approach for osteoporosis since it is independent of other fat types inside the body [10, 28]. Moreover, fat infiltration of muscle (i.e. IMAT) can predict fractures in older adults [14, 29]. High levels of fat infiltration in muscle can have negative impacts on muscle quality and their response to training [30], impaired muscle function [31], and lower physical performance [32]. Hence regular measurement of IMAT and MAT could become of high importance and value in clinical practice.

Compared to other imaging techniques used to quantify muscle and bone mass (i.e., CT and Magnetic Resonance Imaging), DXA quantifies lean mass after subtracting out fat and bone mass, representing an inaccurate measure of muscle mass [33, 34]. Hence, a new image analysis application is needed to accurately estimate muscle, bone, and their components volume in clinical practice. Our application

presents a novel method to measure the volume of musculoskeletal tissues, which correlates with the gold standard (histology) and appears to be fast, simple, valid, and reliable with solid potential for future use in clinical and research settings.

We have also demonstrated that Tissue Compass does not require a large number of sections to accurately quantify bone, muscle, and fat volumes in CT scan images. This is a clear advantage since the radiation exposure will be reduced to a minimum would this method becomes standard practice in the future. In addition, it could become a novel and practical approach to diagnose not only osteoporosis and sarcopenia, but also other tissue loss syndromes associated with cancer, anorexia nervosa, or malnutrition. Future analyses of longitudinal data will be required to quantify the predictive value of Tissue Compass for adverse outcomes in these conditions.

Our validation study has some strengths and limitations. We have compared our software against the most widely used manual image analysis software to quantify MAT and IMAT in research settings. We have also demonstrated that Tissue Compass is a reliable, simple, and fast (Supplementary videos 1 and 2) image analysis method that could be easily translated into clinical practice. However, this study has several limitations. Due to the inherent limitations of image processing techniques, fully automatic segmentation is not possible by our software or any other one, especially for muscle segmentation. However, implementing machine learning protocols and incorporating artificial intelligence (AI) will facilitate full automation of image processing using this software. Implementation of machine learning (ML) may overcome issues with low-quality images as well. Also, we only analyzed images obtained in male subjects. Although a significant difference in the validity of the software in women is unlikely, a study involving female participants, where fat infiltration is more extensive, could still be required.

In summary, this work presents a new application for semiautomatic segmentation and automatic volumetric quantification of medical images. Tissue Compass is a free standalone application specifically developed to assess the structure of musculoskeletal tissues and fat. Implementing AI and ML techniques in both the segmentation process and for further assessment of muscle and bone tissue to predict and diagnose musculoskeletal conditions and tissue loss syndromes is the future scope of the research and development.

Declarations

Acknowledgments: The Osteoporotic Fractures in Men (MrOS) Study is supported by National Institutes of Health funding. The following institutes provide support: the National Institute on Aging (NIA), the National Institute of Arthritis and Musculoskeletal and Skin Diseases (NIAMS), the National Center for

Advancing Translational Sciences (NCATS), and NIH Roadmap for Medical Research under the following grant numbers: U01 AG027810, U01 AG042124, U01 AG042139, U01 AG042140, U01 AG042143, U01 AG042145, U01 AG042168, U01 AR066160, and UL1 TR000128.'

Funding: This study was funded via a Seed Grant from the Australian Institute for Musculoskeletal Science (AIMSS). EB was supported by the Australian Medical Research Frontiers Fund fellowship (MRFF; Melbourne Academic Centre for Health: MACH-RART scheme, 2019).

Author contributions: MI, EBH, and GD contributed to the study design. MI, EBH, ASTNC, SV, and GD contributed to the collection and interpretation of data. All authors contributed to the drafting and critical appraisal of the manuscript and approved the final version.

Conflict of interest: MI, EBH, ASTNC, SV, NEL, JAC, and GD have no conflict of interest to declare.

Ethics statement: All human and animal studies have been approved by the appropriate ethics committee and have therefore been performed following the ethical standards laid down in the 1964 Declaration of Helsinki and its later amendments.

References

1. Kirk B, Zanker J, Bani Hassan E, Bird S, Brennan-Olsen S, Duque G. *Sarcopenia Definitions and Outcomes Consortium (SDOC) Criteria are Strongly Associated With Malnutrition, Depression, Falls, and Fractures in High-Risk Older Persons*. J Am Med Dir Assoc. 2021;**22**:741-745.

2. Soenen S, Chapman IM. *Body weight, anorexia, and undernutrition in older people*. J Am Med Dir Assoc. 2013;**14**:642–8.

3. Greco EA, Pietschmann P, Migliaccio S. *Osteoporosis and Sarcopenia Increase Frailty Syndrome in the Elderly*. Front Endocrinol (Lausanne). 2019;**10**:255.

4. Coll PP, Phu S, Hajjar SH, Kirk B, Duque G, Taxel P. *The prevention of osteoporosis and sarcopenia in older adults*. J Am Geriatr Soc. 2021;**69**(5):1388-1398.

5. Watts, N.B., *Fundamentals, and pitfalls of bone densitometry using dual-energy X-ray absorptiometry (DXA).* Osteoporosis international, 2004. **15**(11): p. 847-854.

6. Bhasin S, Travison TG, Manini TM, Patel S, Pencina KM, Fielding RA, Magaziner JM, Newman AB, Kiel DP, Cooper C, Guralnik JM, Cauley JA, Arai H, Clark BC, Landi F, Schaap LA, Pereira SL, Rooks D, Woo J, Woodhouse LJ, Binder E, Brown T, Shardell M, Xue QL, D'Agostino RB Sr, Orwig D, Gorsicki G, Correa-De-Araujo R, Cawthon PM. *Sarcopenia Definition: The Position Statements of the Sarcopenia Definition and Outcomes Consortium*. J Am Geriatr Soc. 2020;**68**(7):1410-1418.

7. Hirschfeld HP, Kinsella R, Duque G. *Osteosarcopenia: where bone, muscle, and fat collide*. Osteoporos Int. 2017;**28**(10):2781-2790.

8. Bani Hassan, E., et al., *Marrow Adipose Tissue in Older Men: Association with Visceral and Subcutaneous Fat, Bone Volume, Metabolism, and Inflammation.* Calcif Tissue Int, 2018. **103**(2): p. 164-174.

9. Hamrick MW, McGee-Lawrence ME, Frechette DM. *Fatty Infiltration of Skeletal Muscle: Mechanisms and Comparisons with Bone Marrow Adiposity*. Front Endocrinol (Lausanne). 2016;**7**:69.

10. Al Saedi, A., E.B. Hassan, and G. Duque, *The diagnostic role of fat in osteosarcopenia.* J Lab Precis Med, 2019. **4**(7).

11. Scott D, Johansson J, Ebeling PR, Nordstrom P, Nordstrom A. *Adiposity Without Obesity: Associations with Osteoporosis, Sarcopenia, and Falls in the Healthy Ageing Initiative Cohort Study*. Obesity (Silver Spring). 2020;**28**(11):2232-2241.

12. Guerri S, Mercatelli D, Aparisi Gómez MP, Napoli A, Battista G, Guglielmi G, Bazzocchi A. *Quantitative imaging techniques for the assessment of osteoporosis and sarcopenia*. Quant Imaging Med Surg. 2018;**8**(1):60-85.

13. Kim DW, Kim KW, Ko Y, Park T, Khang S, Jeong H, Koo K, Lee J, Kim HK, Ha J, Sung YS, Shin Y. *Assessment of Myosteatosis on Computed Tomography by Automatic Generation of a Muscle Quality Map Using a Web-Based Toolkit: Feasibility Study*. JMIR Med Inform. 2020;**8**(10):e23049.

14. Wong AK, Beattie KA, Min KK, Gordon C, Pickard L, Papaioannou A, Adachi JD; Canadian Multicentre Osteoporosis Study (CaMos) Research Group. *Peripheral quantitative computed tomography-derived muscle density and peripheral magnetic resonance imaging-derived muscle adiposity: precision and associations with fragility fractures in women*. J Musculoskelet Neuronal Interact. 2014;**14**(4):401-10.

15. Wong AK, Chandrakumar A, Whyte R, Reitsma S, Gillick H, Pokhoy A, Papaioannou A, Adachi JD. *Bone Marrow and Muscle Fat Infiltration Are Correlated among Postmenopausal Women With Osteoporosis: The AMBERS Cohort Study*. J Bone Miner Res. 2020;**35**(3):516-527.

16. Hokkanen A, Hämäläinen H, Laitinen TM, Laitinen TP. *Test-Retest Reliability of the Assessment of Fatty Liver Disease Using Low-Dose Computed Tomography in Cardiac Patients*. Front Med (Lausanne). 2021;**8**:656658.

17. Ngo-Huang A, Herbert A, Fontillas RC, Parker NH, Asumbrado R, Garg N, Dibaj S, Liu DD, Ng AH, Guo Y, Shin KY, Katz MHG, Bruera E. *Frequency of Sarcopenia, Sarcopenic Obesity, and Changes in Physical Function in Surgical Oncology Patients Referred for Prehabilitation.* Integr Cancer Ther. 2021;**20**:15347354211000118.

18. Akce M, Liu Y, Zakka K, Martini DJ, Draper A, Alese OB, Shaib WL, Wu C, Wedd JP, Sellers MT, Bilen MA, El-Rayes BF. *Impact of Sarcopenia, BMI, and Inflammatory Biomarkers on Survival in Advanced*

Hepatocellular Carcinoma Treated With Anti-PD-1 Antibody. Am J Clin Oncol. 2021;**44**(2):74-81.

19. Barbalho ER, Rocha IMGD, Medeiros GOC, Friedman R, Fayh APT. *Agreement between software programmes of body composition analyses on abdominal computed tomography scans of obese adults*. Arch Endocrinol Metab. 2020;**64**(1):24-29.

20. Meyer, F., *Topographic distance and watershed lines.* Signal processing, 1994. **38**(1): p. 113-125.

21. Canny, J., *A computational approach to edge detection.* IEEE Transactions on pattern analysis and machine intelligence, 1986(6): p. 679-698.

22. Demontiero, O., et al., *Validation of noninvasive quantification of bone marrow fat volume with microCT in aging rats.* Experimental gerontology, 2011. **46**(6): p. 435-440.

23. Orwoll, E., et al., *Design and baseline characteristics of the osteoporotic fractures in men (MrOS) study—a large observational study of the determinants of fracture in older men.* Contemporary clinical trials, 2005. **26**(5): p. 569-585.

24. Blank, J.B., et al., *Overview of recruitment for the osteoporotic fractures in men study (MrOS).* Contemporary clinical trials, 2005. **26**(5): p. 557-568.

25. Verma, S., et al., *Adipocytic proportion of bone marrow is inversely related to bone formation in osteoporosis.* Journal of clinical pathology, 2002. **55**(9): p. 693-698.

26. Meunier, P., et al., *Osteoporosis and the replacement of cell populations of the marrow by adipose tissue: a quantitative study of 84 iliac bone biopsies.* Clinical Orthopaedics and Related Research (1976-2007), 1971. **80**: p. 147-154.

27. Duque, G., et al., *Age-related bone loss in the LOU/c rat model of healthy ageing.* Experimental gerontology, 2009. **44**(3): p. 183-189.

28. Singh L, Tyagi S, Myers D, Duque G. Good, Bad, or Ugly: the Biological Roles of Bone Marrow Fat. Curr Osteoporos Rep. 2018;**16**(2):130-137.

29. Schafer, A.L., et al., *Fat infiltration of muscle, diabetes, and clinical fracture risk in older adults.* The Journal of Clinical Endocrinology & Metabolism, 2010. **95**(11): p. E368-E372.

30. Marcus, R.L., O. Addison, and P.C. LaStayo, *Intramuscular adipose tissue attenuates gains in muscle quality in older adults at high risk for falling. A brief report.* The journal of nutrition, health & aging, 2013. **17**(3): p. 215-218.

31. Robles, P.G., et al., *Intramuscular Fat Infiltration Contributes to Impaired Muscle Function in COPD.* Medicine and Science in Sports and Exercise, 2015. **47**(7): p. 1334-1341.

32. Therkelsen, K.E., et al., *Intramuscular fat and physical performance at the Framingham Heart Study.* Age, 2016. **38**(2): p. 31.

33. Levine, J.A., et al., *Measuring leg muscle and fat mass in humans: comparison of CT and dual-energy X-ray absorptiometry.* Journal of Applied Physiology, 2000. **88**(2): p. 452-456.

34. Maden-Wilkinson, T., et al., *Comparison of MRI and DXA to measure muscle size and age-related atrophy in thigh muscles.* Journal of musculoskeletal & neuronal interactions, 2013. **13**(3): p. 320-8.

Tables

Table 1 *– Comparison of measurements of Tissue Compass™ and SliceOmatic of MAT, HBM, and bone in rat femur micro-CT scans.*

Area of Study	Correlation coefficient	Bland Altman mean difference and limits of agreement	Individual ICC (95% CI)
MAT in Rat femur	0.992	-720.89 (-1.5e+04, 13074.00)	0.99 (0.98, 1.00)
HBM in Rat femur	0.938	4421.11 (-1.8e+04, 27149.73)	0.93 (0.81, 0.97)
Bone in Rat femur	0.971	-6073.32 (-2.9e+04, 16388.37)	0.97 (0.90, 0.99)

Number of rat femur Micro-CT scans = 19

Table 2 *– Comparison of MAT, HBM, and bone measurements in the left hip and L1 vertebra from two observers using Tissue Compass™.*

Area of Study	Correlation coefficient	Bland Altman mean difference and limits of agreement	Individual ICC (95% CI)
MAT in Left Hip	1	0.01 (-0.07, 0.10)	1.00 (1.00, 1.00)
HBM in Left Hip	1	0.02 (-0.08, 0.12)	1.00 (1.00, 1.00)
Bone in Left Hip	1	0.05 (-0.15, 0.25)	1.00 (1.00, 1.00)
MAT in L1 Vertebra	1	0.02 (-0.18, 0.22)	1.00 (1.00, 1.00)
HBM in L1 Vertebra	0.999	0.00 (-0.16, 0.16)	1.00 (1.00, 1.00)
Bone in L1 Vertebra	0.999	0.02 (-0.23, 0.27)	1.00 (1.00, 1.00)

Number of QCT scans = 50

Table 3 *– Comparison of Tissue Compass™ and SliceOmatic measurements of MAT, HBM, and bone in the left hip and L1 vertebra and muscle and IMAT in the psoas muscle.*

Area of study	Correlation coefficient	Bland Altman mean difference and limits of agreement	Individual ICC (95% CI)
MAT in Left Hip	1	0.03 (-0.13, 0.20)	1.00 (1.00, 1.00)
HBM in Left Hip	0.999	0.05 (-0.08, 0.18)	1.00 (0.99, 1.00)
Bone in Left Hip	1	0.05 (-0.24, 0.34)	1.00 (1.00, 1.00)
MAT in L1 Vertebra	0.999	-0.02 (-0.34, 0.31)	1.00 (1.00, 1.00)
HBM in L1 Vertebra	0.997	-0.14 (-0.44, 0.17)	0.99 (0.97, 1.00)
Bone in L1 Vertebra	0.998	-0.29 (-0.62, 0.05)	0.99 (0.64, 1.00)
IMAT in Psoas	0.995	0.03 (-0.08, 0.15)	0.99 (0.99, 1.00)
Muscle in Psoas	0.996	0.02 (-0.35, 0.38)	1.00 (0.99, 1.00)

Number of QCT scans = 100

Figures

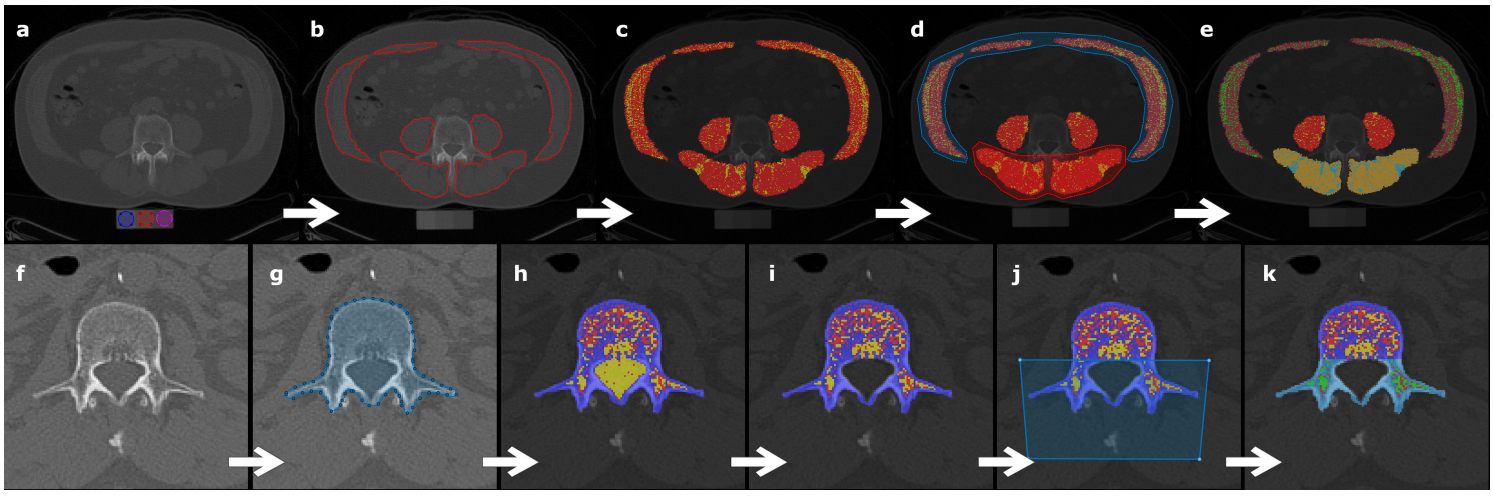

Figure 1

Example of the steps involved in segmentation and labeling of muscle and bone using Tissue Compass. The main steps for muscle analysis are: a,b)segmentation and removal of non-target tissues, c) labeling, d, e) masking (optional). The main steps involved in bone analysis are: f, g) segmentation and ROI editing, h)labeling, i)spinal cord elimination (automatic and optional), j, k) masking (optional).

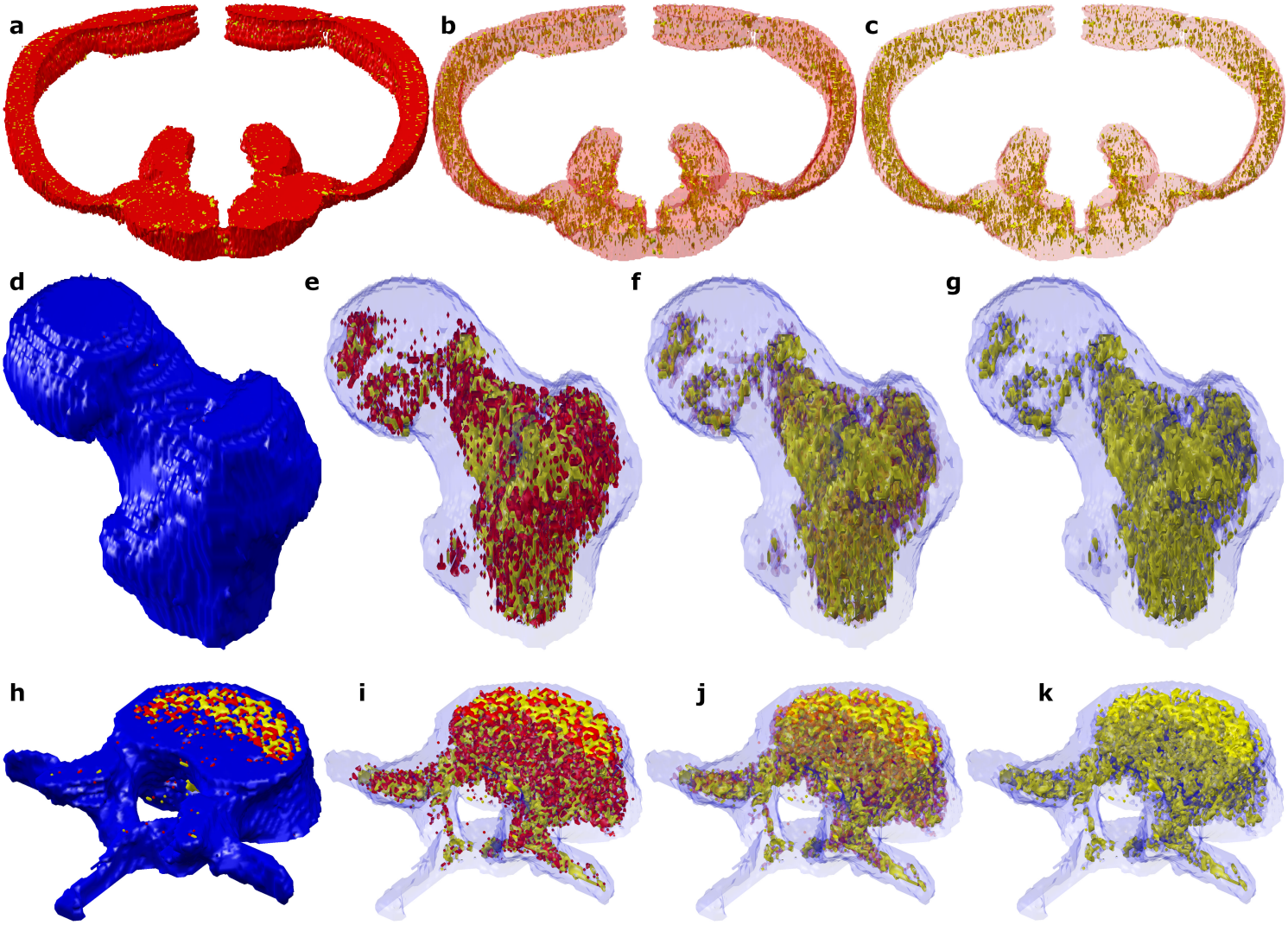

Figure 2

Example of 3D visualization of images with different levels of transparency using Tissue Compass™ in three separate areas of study: a-c) abdominal muscle at the L4 level. The colors red and yellow represent muscle and IMAT, respectively. d-g) L1 vertebra, h-k) Left hip. Colors blue, red and yellow for the L1 vertebra and left hip represents bone, HBM, and MAT, respectively.

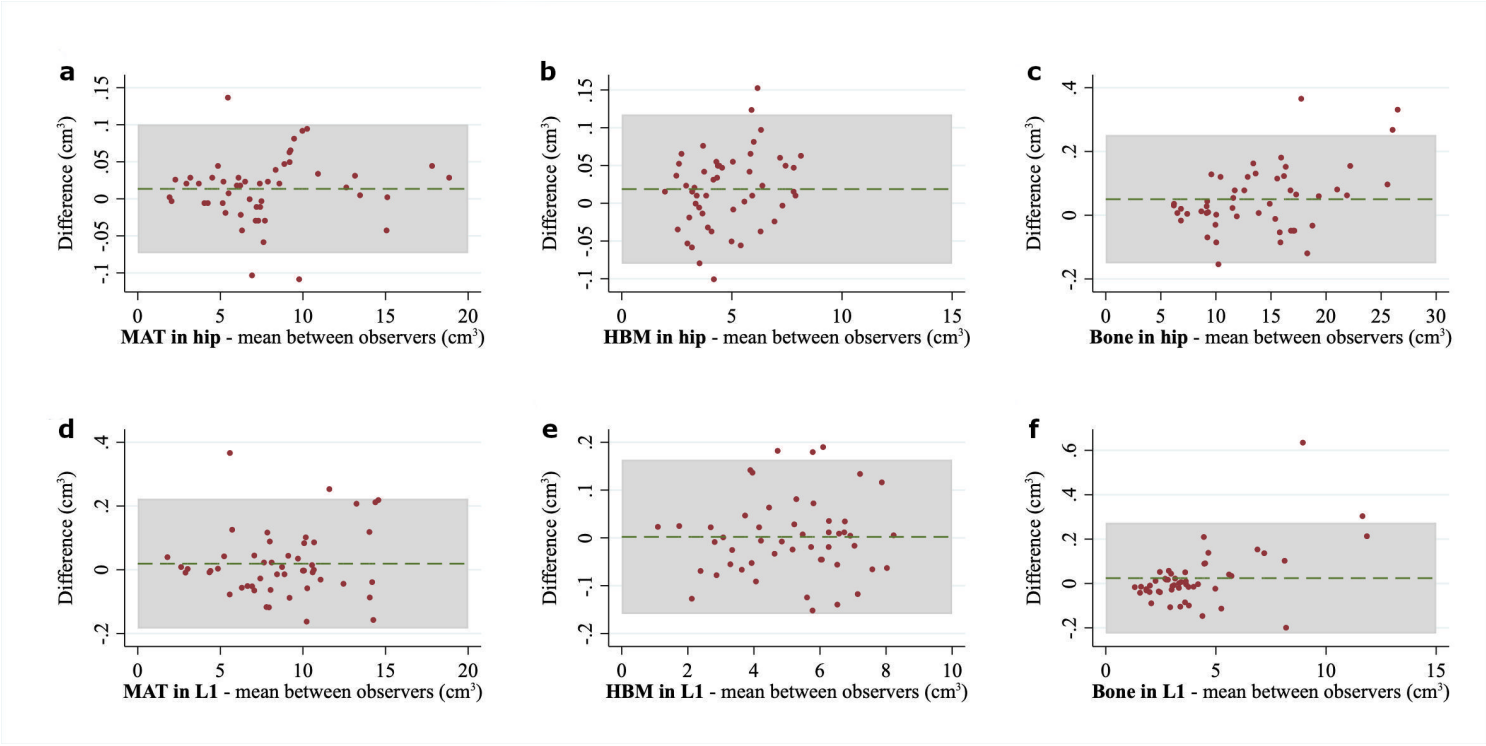

Figure 3

Agreement between two observers using Tissue Compass™ for MAT, HBM, and bone in a-c) Left hip d-f) L1 vertebra. The difference in the plots is the difference between the two observers.

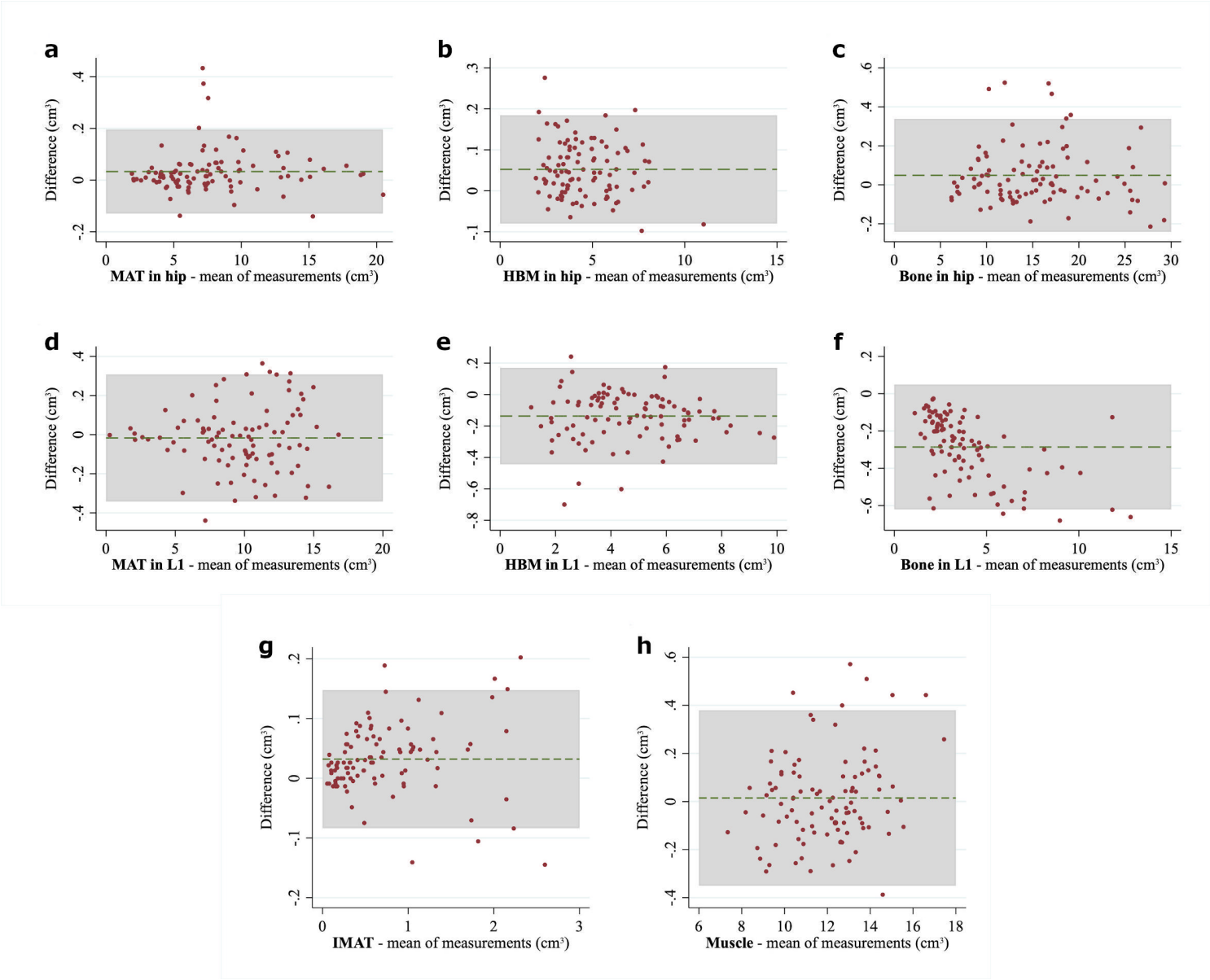

Figure 4

Agreement between methods (SliceOmatic vs. Tissue Compass™) for MAT, HBM, and bone volume in a-c) left hip, d-f) L1 vertebra, and g, h) muscle and IMAT in psoas muscle (L4 level). The difference in the plots is the difference between Tissue Compass™ and SliceOmatic.

Supplementary Files

This is a list of supplementary files associated with this preprint. Click to download.

- Supplementalfigure2.tiff
- Supplementalfigure1.tiff
- supplement1.mp4
- supplement2.mp4